

# A LARGE NUMBER OF $Z > 6$ GALAXIES AROUND A QSO AT $Z = 6.43$ : EVIDENCE FOR A PROTOCLUSTER?

YOUSUKE UTSUMI

The Graduate University for Advanced Studies, 2-21-1 Osawa Mitaka Tokyo, Japan and  
National Astronomical Observatory of Japan, 2-21-1 Osawa Mitaka Tokyo, Japan

TOMOTSUGU GOTO

Institute for Astronomy, University of Hawaii and  
Subaru Telescope 650 North A'ohoku Place Hilo, HI 96720, USA

NOBUNARI KASHIKAWA, SATOSHI MIYAZAKI, AND YUTAKA KOMIYAMA

The Graduate University for Advanced Studies, 2-21-1 Osawa Mitaka Tokyo, Japan and  
National Astronomical Observatory of Japan, 2-21-1 Osawa Mitaka Tokyo, Japan

HISANORI FURUSAWA

National Astronomical Observatory of Japan, 2-21-1 Osawa Mitaka Tokyo, Japan

RODERIK OVERZIER

Max-Planck Institut für Astrophysik, D-85741 Garching, Germany  
*Draft version August 20, 2018*

## ABSTRACT

QSOs have been thought to be important for tracing highly biased regions in the early universe, from which the present-day massive galaxies and galaxy clusters formed. While overdensities of star-forming galaxies have been found around QSOs at  $2 < z < 5$ , the case for excess galaxy clustering around QSOs at  $z > 6$  is less clear. Previous studies with HST have reported the detection of small excesses of faint dropout galaxies in some QSO fields, but these surveys probed a relatively small region surrounding the QSOs. To overcome this problem, we have observed the most distant QSO at  $z = 6.4$  using the large field of view of the Suprime-Cam ( $34' \times 27'$ ). Newly-installed red-sensitive fully depleted CCDs allowed us to select Lyman break galaxies (LBG) at  $z \sim 6.4$  more efficiently. We found seven LBGs in the QSO field, whereas only one exists in a comparison field. The significance of this apparent excess is difficult to quantify without spectroscopic confirmation and additional control fields. The Poisson probability to find seven objects when one expects four is  $\sim 10\%$ , while the probability to find seven objects in one field and only one in the other is less than  $0.4\%$ , suggesting that the QSO field is significantly overdense relative to the control field. These conclusions are supported by a comparison with a cosmological SPH simulation which includes the higher order clustering of galaxies. We find some evidence that the LBGs are distributed in a ring-like shape centered on the QSO with a radius of  $\sim 3$  Mpc. There are no candidate LBGs within 2 Mpc from the QSO, i.e., galaxies are clustered around the QSO but appear to avoid the very center. These results suggest that the QSO is embedded in an overdense region when defined on a sufficiently large scale (i.e. larger than an HST/ACS pointing). This suggests that the QSO was indeed born in a massive halo. The central deficit of galaxies may indicate that (1) the strong UV radiation from the QSO suppressed galaxy formation in its vicinity, or (2) that star-formation closest to the QSO occurs mostly in an obscured mode that is missed by our UV selection.

## 1. INTRODUCTION

At  $2 < z < 5$ , strong overdensities of star-forming galaxies have been found around QSOs and radio galaxies, and thus, QSOs have been thought to trace highly biased regions in which the present-day massive galaxy clusters formed (e.g. Djorgovski et al. 2003; Miley et al. 2004; Kashikawa et al. 2007). It is expected that this extends to the most luminous  $z \sim 6$  QSOs as well, as this rare population hosts supermassive black holes of several

billion solar masses that are presumed to reside in the most massive galaxies and dark matter halos present at this redshift.

However observational results to date have been puzzling; Five  $z \sim 6$  QSO fields observed by the HST/ACS show no major enhancements in the galaxy density (Kim et al. 2009). Even though a few QSO fields have showed an apparent overdensity (Stiavelli et al. 2005; Zheng et al. 2006), none of them were among the richest structures discovered to date at  $z \sim 6$ , as evidenced by much larger overdensities found in random fields (e.g., Ouchi et al. 2004b; Kashikawa et al. 2007;

Based on data collected at Subaru Telescope, which is operated by the National Astronomical Observatory of Japan.  
yousuke.utsumi@nao.ac.jp

Ota et al. 2008, see Overzier et al. (2009) for a discussion).

Why do QSOs suddenly appear to stop being at the center of the overdensity at  $z \sim 6$ ? One hypothesis is that despite the higher dark matter densities near the QSOs, the strong ionizing UV radiation from the central QSOs may prohibit the condensation of gas thereby suppressing galaxy formation around the QSOs (Barkana & Loeb 1999). An alternative and perhaps more likely explanation is that the lack of overdensities identified is related to the fact that it is currently technically challenging to perform a survey deep enough to detect faint  $z \sim 6$  galaxies and cover an area large enough to probe the large-scale structure surrounding the QSOs.

In this work, we aim to study the large scale structure around the currently most distant QSO at  $z = 6.43$ , taking advantage of the large aperture of the 8.2m telescope ‘‘Subaru’’ located on Maunakea Observatory and the wide field prime focus camera ‘‘Suprime-Cam’’ ( $34' \times 27'$ ) (Miyazaki et al. 2002b). In addition, we have recently installed new red-sensitive fully depleted CCDs on the Suprime-Cam (Kamata et al. 2008), allowing us to reach necessary depths in much shorter exposure time. Improved sensitivity is a factor of about 1.4 and 2 better in the  $z'$ -band and at  $\sim 1\mu\text{m}$ , respectively.

Throughout the paper, we use  $H_0 = 70h_{70} \text{ km s}^{-1} \text{ Mpc}^{-1}$ ,  $\Omega_m = 0.3$ ,  $\Omega_\Lambda = 0.7$ . Magnitudes are given in the AB system.

## 2. DATA & ANALYSIS

### 2.1. Observation

We observed the field surrounding the most distant QSO, CFHQSJ2329-0301 at  $z = 6.43$ ,  $M_{1450} = -25.23$  (Willott et al. 2007) using Suprime-Cam with the filters  $i'$ ,  $z'$ ,  $z_R$  during an engineering run in Aug 2008 and UH time in Jun 2009. We used the special  $z_R$  band filter constructed by Shimasaku et al. (2005). This filter covers the redder side of the  $z'$  band and has a central wavelength of  $9900\text{\AA}$  (Fig.1). The seeing was stable throughout the runs, with a FWHM  $\approx 0.5$  arcsec in  $i'$ ,  $0.4 \sim 0.7$  arcsec in  $z'$  and  $0.5 \sim 0.7$  arcsec in  $z_R$ . The exposure times were 360 and 500 s in  $i'$  and  $z_R$ , respectively. The exposure times in the  $z'$  band varied; we obtained 3 exposures of 100 s, 2 of 300 s, 3 of 400 s, 6 of 500, and 2 of 700 s resulting in more than 10000 ADU of sky counts. The total exposure time in  $i'$ ,  $z'$  and  $z_R$  were 3,600 s on Aug 28 2008, 6,900 s on 2, Aug 27 and 12,532 s on Aug 27 2008 and Jun 18 2009 respectively, under good seeing conditions (less than 0.6 arcsec FWHM). Our dither strategy consisted of five or more pointings on a circle of 1 arcmin radius.

### 2.2. Data Reduction

Our reduction procedure follows Miyazaki et al. (2002a), with small adjustments made related to the new CCD. A major difference between the old and new Suprime-Cam is that the latter has 4 channel read out circuits for faster readout. As a result, over-scan subtraction and background sky-subtraction should be performed on each channel individually for each CCD. An overscan value is evaluated by taking the mean along the columns of the overscan region of each channel, and then subtracted from the science region. A flat field image is

created by taking the median of all science images after masking objects. The background sky is subtracted on each channel after flat fielding. To estimate the background, we first reject data points having 2 times larger or 4 times lower sigma value than the sky value. The upper cut prevents astronomical objects from contaminating the sky, while the lower cut removes residuals from the flat-fielding. Then, we estimate the modes in  $64 \text{ pixel} \times 64 \text{ pixel}$  boxes. A background of each pixel is estimated by interpolating these mode values at vertexes of a triangle centered on the pixel.

Before combining all the science frames, the images need to be corrected for (1) geometric distortion, (2) displacement and rotation of each CCD from the fiducial position, and (3) pointing offsets between exposures. We corrected for these effects by minimizing the positional differences of common control stars identified on each CCD in all exposures relative to the first exposure. The resulting positional error of the control stars from the fiducial point is approximately 0.5 pixel (rms). We solve the transformation among the 3 bands, aligning each frame with the first exposure of the  $z_R$  band in order to perform multi-band photometry using an aperture as small as possible to obtain a high S/N ratio. Flux offsets are also calculated during this procedure. Since we want to determine the transformation among the bands as accurately as possible, an image warping procedure was performed only once, and a second order bi-linear interpolation was used for rebinning. For stacking, we adopted the clipped mean in order to eliminate cosmic rays. The implementation of these reduction steps were performed using the software suite *imcat*.

### 2.3. Photometric Calibration

Photometric calibration is performed by comparing stars in a reference field 2 deg away to the North  $(\alpha, \delta)_{2000} = (23 : 29, -01 : 01)$  with those in the SDSS/DR7 star catalog (Abazajian & Sloan Digital Sky Survey 2008) and using the following equations:

$$i'_{\text{Subaru}} = 0.125(i' - r')_{\text{SDSS}} + 0.003 + i'_{\text{SDSS}} \quad (1)$$

$$z'_{\text{Subaru}} = -1.091(i' - z')_{\text{SDSS}} + 0.004 + i'_{\text{SDSS}} \quad (2)$$

$$z_{R, \text{Subaru}} = -1.414(i' - z')_{\text{SDSS}} + 0.021 + i'_{\text{SDSS}} \quad (3)$$

These equations are determined from Gunn & Stryker (1983) and convolved with response curves that include both optics and the atmosphere. We measured the efficiency of the new CCDs in Kamata et al. (2008). Since the calibration field was observed soon after the completion of our science exposure, no airmass/atmospheric corrections were needed to obtain the photometric zero-point. After the correction, the rms of the magnitude differences between our catalog and the SDSS catalog are 0.06, 0.07 and 0.07 in  $i'$ ,  $z'$  and  $z_R$ , respectively.

We have checked the colors of a sample of star-like objects selected according to `CLASS_STAR > 0.9`, by comparing the color of the stars from Gunn & Stryker (1983) to the observed ones, confirming a good internal consistency of colors in our catalog. The template and observed colors were consistent within an accuracy of 0.05 mag. Since the seeing in the final images are 0.58, 0.54 and 0.50 arcsec (FWHM), we use a small aperture to perform photometry to obtain a better S/N ratio. Fol-

lowing Shimasaku et al. (2005), who used an aperture size twice that of PSF, we adopt a 1.2 arcsec aperture to perform photometry. The 3 sigma limiting magnitudes within this 1.2 arcsec aperture are  $i' = 26.95$ ,  $z' = 26.13$ , and  $z_R = 25.46$  (AB) mag. Here,  $1\sigma$  sky magnitudes are computed by randomly placing a 1.2 arcsec aperture in the blank (sky) part of each image (Yagi et al. 2002; Ouchi et al. 2004a).

#### 2.4. Astrometric Calibration

We obtain an astrometric solution by comparing our catalog with the USNO-B1.0 catalog (see *scamp* (Bertin 2006)). The resulting accuracy of the astrometric solution is 0.5 arcsec (rms). Note that we did not use this astrometric solution to stack individual raw images, but only to obtain the final absolute positions of the objects.

#### 2.5. Object Detection

The object detection is performed by SExtractor 2.3.2 (Bertin & Arnouts 1996). We constructed a detection image, the “all”- $z_R$  image, by combining all science frames, including those with a slightly poorer seeing conditions. The object detection reliability using this “all”- $z_R$  image is higher than when only using the  $z_R$  image for detection given that  $\approx 3\sigma$  sources in the  $z_R$  image are detected at  $\approx 3.7\sigma$  in the “all”- $z_R$  image. Using the “all”- $z_R$  image, we consider an object detected if it has more than 5 connected pixels with each exceeding the local sky rms by a factor of 2. To reduce contamination by false detections, we only use the “detected cleanly” and “no blending” objects that have `FLAGS=0` in SExtractor. We measure the magnitudes in 1.2 arcsec apertures for each pass-band to derive colors of the detected objects, and adopted `MAG_AUTO` as our estimate for the total  $z_R$  magnitude. Objects in the  $i'$ -band fainter than 2 sigma were replaced by the 2 sigma limiting magnitude as an upper limit. In addition, all objects having detections in the  $z'$ -band of less than  $2\sigma$  were rejected in order to keep spurious detection at a minimum.

Some lower S/N regions, such as the “blooming regions” (the halos and horizontal spikes surrounding bright stars), as well as the outer edge of the image, are masked manually. The resulting effective field of view is  $0.219\text{ deg}^2$ . We detect 48,632 objects after masking (to a limiting magnitude of 25.46, or 3.7 sigma detections on the “all”- $z_R$  image). The number of detections is comparable to that in our comparison field, the Subaru deep field (SDF), which contains 45,405 objects in a single field of view of the Suprime-Cam (Shimasaku et al. 2005).

#### 2.6. SED Modeling

We have upgraded the CCDs of the Suprime-Cam to red-sensitive ones, which have 1.4 and 2 times better sensitivity in  $z'$  and  $z_R$  compared to the previous detectors. Thus, we can reach the necessary depth in much shorter exposure time. This improved sensitivity allows us to efficiently use the  $z' - z_R$  color to select Lyman break galaxies at  $z > 6.4$ . At the QSO redshift of  $z = 6.43$ , the  $z' - z_R$  color selection is more efficient in selecting galaxies than the  $i' - z'$  color selection (the so-called  $i$ -dropout technique), which has been used in previous works to select  $5.5 < z < 6.5$  galaxies (Fig.1).

In order to predict the colors of galaxies as a function of their redshift, we computed  $z' - z_R$  colors of model galax-

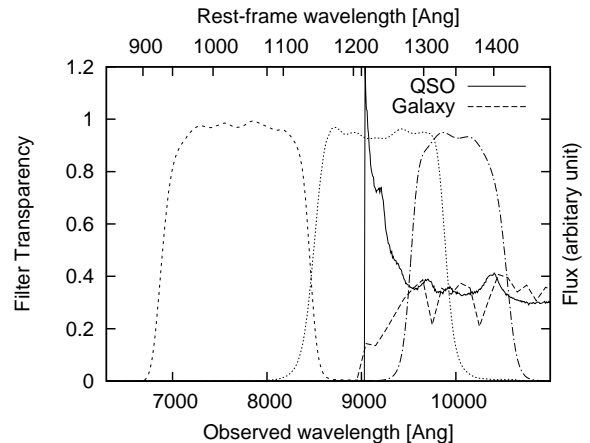


FIG. 1.— An example of the spectra of a galaxy and a QSO redshifted to  $z = 6.43$ . The filter response curves in  $i'$ ,  $z'$  and  $z_R$  are indicated from left to right. The spectrum of the galaxy is based on a model having an exponentially-declining star formation history and an age of 0.5 Gyr (Bruzual & Charlot 2003), while the spectrum of the QSO is based on the QSO composite spectrum taken from (Vanden Berk, D. E. et al. 2001).

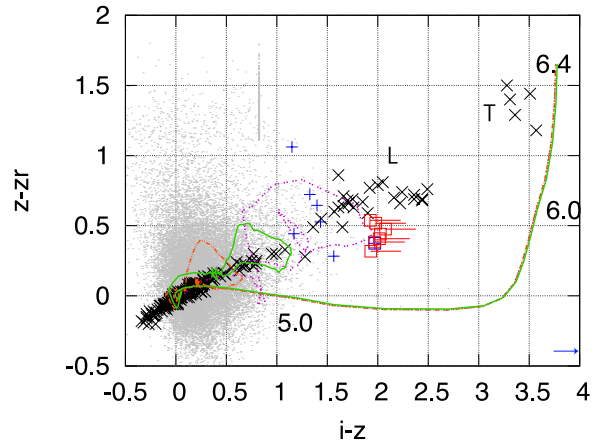


FIG. 2.—  $i' - z'$  vs  $z' - z_R$  color-color diagram, showing the locations of detected objects, candidate  $z \sim 6.4$  galaxies, stellar objects, and tracks indicating the expected colors of low- and high redshift galaxies. Gray dots are all objects fainter than  $z_R = 24.0$ . Red squares are  $z \sim 6.4$  galaxies selected in the QSO field. Blue pluses are objects detected as  $z \approx 6$  galaxies in Shimasaku et al. (2005) in the SDF. Gray box crosses are stars (Gunn & Stryker 1983; Chiu et al. 2006; Golimowski et al. 2004; Knapp et al. 2004). The purple, green, and orange lines represent model galaxies having star formation histories (Bruzual & Charlot 2003). Absorption by the neutral hydrogen at each redshift was added following the prescription of Fan et al. (2006a). The blue arrow indicates CFHQS J2329-0301 (see Table 2).

ies (0.05, 0.1, 0.2 Gyr of age, using Bruzual & Charlot (2003)) and added the absorption effects from the neutral hydrogen in the intergalactic medium (Fan et al. 2006a). According to our modeling, colors of  $i - z' > 1.9$  and  $z' - z_R > 0.3$  can be used to identify galaxies at  $z > 5.8$  (Fig. 2).

#### 2.7. Object Selection

Here we will select LBGs at  $z > 6.4$  using our  $i'$ ,  $z'$ ,  $z_R$  catalog. The model colors shown in Fig. 2 predicts that galaxies at  $z = 6.4$  should have a large color difference of about  $i' - z' \simeq 3.5$ . However, for an object having  $z' \simeq 25$  this would require  $i' \simeq 28.5$  mag, much fainter than our

detection limits. Therefore, we slightly loosen the color cut and require  $i' - z' > 1.9$  and  $z' - z_R > 0.3$ . These relaxed criteria are still appropriate for selecting LBGs at  $z > 6.4$ , although we must be somewhat cautious of potential galaxies at  $z \simeq 1.8$  having colors of  $i' - z' \simeq 1.9$  that could make it into the sample as well. In order to assess the impact of this effect on our conclusions, in section 3.3 below we will try to statistically estimate the number of such  $z \simeq 1.8$  interlopers expected.

In our control field (the SDF), only a single object was found that satisfied our color criteria, and this object was classified as a genuine  $z \sim 6$  galaxy by Shimasaku et al. (2005). Because the SDF data are deeper than ours, we adjusted the depth of that field by replacing the magnitudes of all objects fainter than our limits with the limiting magnitudes as computed for our field. We also removed two objects brighter than  $z_{R,Auto} = 24.0$  since such objects are too bright to be at  $z = 6.4$  (according to a  $z \sim 6$  LBG study in the SDF, there is no  $z > 6$  galaxy brighter than  $z_R = 24.8$ , see Shimasaku et al. (2005)). These two objects may be contaminating stars since they have SExtractor CLASS\_STAR values greater than 0.95, meaning that they are likely to be unresolved.

As a result, to the magnitude limit of  $z' < 25.46$ , we have detected 7 objects that are good candidates for being  $z \sim 6$  LBGs. These objects are shown as red squares in Fig. 2. Note that the (lower limits on) their  $i - z$  colors are bluer than expected from the models, due to the relatively shallow limiting magnitude in  $i'$ .

### 3. SOURCES OF CONTAMINATION

#### 3.1. False Detections

Because we are selecting very faint objects, our sample may be contaminated by false detections due to background fluctuations. To evaluate the number of such contaminations, we created a negative of the “all”- $z_R$  image, and repeated our detection, photometry and masking routines on each of the filter images. No detections were obtained based on this negative image. We conclude that our catalog is not affected by spurious detection.

#### 3.2. Contamination by Faint Dwarf Stars

As we can see in Fig. 2, L/T dwarf stars also satisfy our adopted color cut ( $i' - z' > 1.9$  &  $z' - z_R > 0.3$ ). In this subsection, we estimate the expected number of L and T dwarfs, given the size, depth and Galactic position of the field.

As a first test, when we applied our color criteria to the SDF only one object was found and classified as a genuine  $z \sim 6$  object (see above). The second reddest object in the field has  $i - z \sim 1.65$ , i.e., there are no stellar-like objects in the SDF with colors red enough to make it into our selection.

However, we need to take into account the different galactic latitudes of our field and the SDF. Unfortunately, the late-type star counts as a function of Galactic position are not accurately known at the faint magnitudes we are probing. Late-type stars having similar colors to high- $z$  galaxies can only be distinguished by using deep spectroscopic observations. The latest estimate was performed by Caballero et al. (2008), who studied the contamination from L, T dwarfs by modeling the spatial distribution of late type stars in the

Galactic thin disc described using an exponential law  $n_i = n_{A,i} e^{-\frac{d}{d_B(l,b)}}$ ,  $\frac{1}{d_B} \equiv \frac{\cos b \cos l}{h_R} \pm \frac{\sin b}{h_Z}$ , where  $n_{A,i}$  is the number density of  $i$ -type stars,  $h_R$ ,  $h_Z$  are the scale length and the scale height of the exponential disc and  $d$  is the distance to us in galactic coordinates,  $d = (R_\odot^2 + d^2 \cos^2 b - 2R_\odot d \cos b \cos l)^{1/2}$ . The adopted parameters are  $R = 8.6\text{kpc}$ ,  $h_R = 2.25\text{kpc}$ ,  $h_Z = 0.3\text{kpc}$ . Local spatial densities of late type stars are adopted from a compilation given in Caballero et al. (2008), while relations between the type and absolute magnitude are taken from Knapp et al. (2004). According to this model calculation, we expect 1.5 times as many L/T dwarfs as in the SDF for  $z_R < 25.25$  mag, corresponding to the faintest bin of the magnitude of our selected objects.

We have seen that there were no stars in our  $z \sim 6.4$  color-selection in the SDF. Here we try to scale that null detection in the SDF to our field. If we assume that stars follow a Poisson distribution, the expected number of L/T dwarfs in the SDF is 0.40 per field at a 68% confidence level. Using the Galactic scaling computed above, we expect that the probability of finding two or less stars in our field is 87%. Given that we have already rejected two stellar like objects (§2.5), the chance of finding one more star is less than two%. Therefore, we conclude that there is little chance that our  $z \sim 6.4$  LBG catalog is contaminated by stellar objects. We note, however, that object with id 1 could be a dwarf star since its  $i' - z'$  color is not large enough. We will include this object in the following discussion.

#### 3.3. Contamination by red galaxies at $z \sim 1.8$

As mentioned earlier, we found only one object when applying our adopted color criteria for  $z \sim 6.4$  galaxies to the SDF catalog (after adjusting the limiting magnitudes to ours), and this object was identified as a  $z \sim 6$  object given that its  $B, V, R$  magnitudes were too faint for a low- $z$  interloper. Based on this, the expected number of  $z \sim 1.8$  galaxies found according to our criteria should be close to zero with an upper limit of 1.83 at a confidence level of 84% (Gehrels 1986). Although cosmic variance should ideally be taken into account as well, we do not have any other suitable comparison fields that are as deep in  $z_R$  as the SDF.

However, we use the publicly available SXDS DR1 catalog (Furusawa et al. 2008) to obtain a rough estimate of the expected contamination using only a  $i - z > 1.9$  color cut. The SXDS covers 5 pointings with the Suprimecam, and thus, the cosmic variance is less of a concern. We first applied again the observational limits as given by our field by replacing all magnitudes that are fainter than our limiting magnitudes ( $i'_{2\sigma} = 27.39$ ,  $z'_{2\sigma} = 26.57$ ) by our  $2\sigma$  upper limits. We used FLAG=0 in order to select only cleanly detected objects, and trimmed a region of lower S/N (500 pixels from the edge of the field). Only 3 objects were found that passed the selection criteria in all 5 pointings of the SXDF. These objects are detected in the  $B$  band (brighter than 28.4,  $3\sigma$  mag), indicating that they are most likely low redshift interlopers at a redshift of  $z \sim 1.8$ . If we scale this number to the area of our single pointing field, only 0.6 of such interlopers are galaxies are expected in our. This rough estimate is consistent with the estimate derived above based on the SDF, suggesting that the contamination from  $z \sim 1.8$

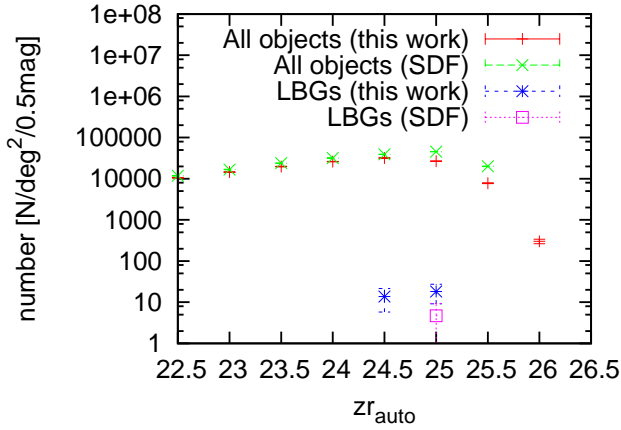


FIG. 3.— Number counts of all detected objects and the  $z$ -dropout galaxies. We did not apply completeness corrections. The number of LBGs in our field is larger than that in the SDF although the opposite is true when comparing the total number of 1 detected objects.

galaxies is negligible.

#### 4. RESULTS

##### 4.1. Number Counts

Fig. 3 shows the number counts of all detected objects, as well as those of the  $z \sim 6$  galaxies. The number of all objects in this field is slightly lower, by about 20%, than those detected in the SDF field at  $z_R < 24$ . This could be due to a small difference in the absolute photometric calibrations between the two catalogs, or due to cosmic variance. If it were due to a difference in photometric calibration, a shift of 0.2 magnitude would be required to explain the difference. Note that such an offset, if real, would not affect the colors used in our color selection of the  $z \sim 6$  galaxies, as the colors were checked for internal consistency using a catalog of stars. We next consider the possibility of cosmic variance. Furusawa et al. (2008) observed five Suprime-Cam pointings and derived the number counts. The variance in the number counts was found to amount to a factor of 1.7 among the individual pointings in the  $z'$  band. Thus, we conclude that the differences in the number counts found between our field and the SDF are consistent with being due to cosmic variance. Finally, we note that at magnitudes fainter than  $z_R = 25$  the difference in number counts becomes larger again, but this is simply because our data are slightly shallower than the SDF.

##### 4.2. Comparing the LBG number density in the QSO field with that in the SDF

We detect 7 objects as  $z \sim 6.4$  galaxy candidates using the color criteria in § 2.7, while 9 objects are rejected as lower redshift objects at  $z < 5.5$  based on a  $z' - z_R$  color cut (it would have been difficult to eliminate these objects using only  $i' - z'$ ). For comparison, we apply the same color criteria to the SDF catalog after applying our magnitude limits and find only one candidate. Thus the number of  $z \sim 6.4$  galaxies in the QSO field is 7 times larger than that the SDF field. We note that if we apply a more relaxed cut based on a single color of  $i - z > 1.9$  (the standard  $i$ -dropout technique) to the reference field (SDF), we still find 4 objects although 16 objects found

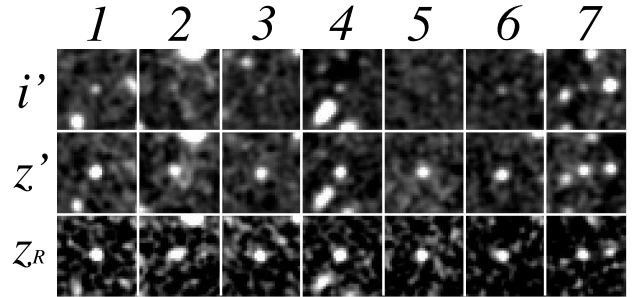


FIG. 4.— Thumbnail images of the LBG candidates in the QSO field. The properties of the individual sources are listed in Table 1.

in the QSO field, implying that even with the standard  $i$  dropout technique we find an overdensity in the QSO field.

The properties of the objects identified are summarized in Table 1, and we show the filter thumbnail images in Fig. 4. Although our data are shallower than the SDF, we have detected more LBGs than in the SDF. The result suggests that the number density of  $z \sim 6.4$  galaxies in this QSO field is larger than that in the SDF field. Such an overdensity would be consistent with the predictions from cosmological simulations (e.g., Springel et al. (2005)) that suggest that the first QSOs are situated in the most prominent dark matter haloes and are surrounded by a large number of fainter galaxies. Although the redshift discrimination offered by our photometric selection is not very accurate, the chance of finding a random projection of seven galaxies at  $z \sim 6 - 7$  is quite unlikely given their overall low number density. We speculate that we are seeing the most distant proto-cluster centered on a massive QSO at  $z = 6.43$ .

##### 4.3. Assessing the significance of the overdensity

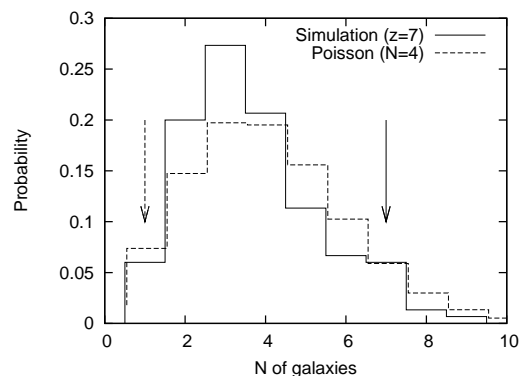


FIG. 5.— The probability distribution of how many galaxies would be found within the field of view of Suprime-Cam using our selection criteria. The solid histogram is based on the simulation of galaxy formation at  $z = 7$  while the dashed histogram is the Poisson distribution assuming the average value is  $(7 + 1)/2 = 4$ . The solid and the dashed arrows indicate the number of galaxies in the QSO field and the SDF comparison field, respectively.

In this subsection, we assess how significant the overdensity is. If we assume a Poissonian distribution, the probability of finding seven objects when one expects one (based on the SDF counts) is less than 0.01%. However this is not a fair statistic since we have only one comparison field (the SDF) which has a similar size as the

TABLE 1  
THE PROPERTIES OF THE  $z \sim 6.4$  CANDIDATE GALAXIES DETECTED  
IN THE QSO FIELD.

id	$\alpha_{2000}$	$\delta_{2000}$	$z_R$	$i' - z'$	$z' - z_R$	FWHM
1	23:29:20.56	-02:54:29.5	24.62	2.03	0.44	0.63
2	23:29:24.10	-03:07:34.3	24.64	> 1.93	0.54	1.15
3	23:29:28.56	-02:57:38.4	24.69	> 1.98	0.52	0.55
4	23:28:48.69	-03:06:23.3	24.88	> 2.08	0.48	0.58
5	23:28:58.68	-03:12:11.6	24.98	> 2.02	0.41	0.64
6	23:30:04.24	-02:56:54.6	25.00	> 1.97	0.38	0.69
7	23:29:31.52	-03:11:05.0	25.11	> 1.93	0.32	1.02

QSO field. If we naively calculate the average number of counts expected from the two fields combined,  $(7+1)/2$ , we expect 4 counts on average. The Poissonian probability to find 7 objects is thus  $\sim 11\%$ . However, the chance of finding one object in one field and seven in the other is much lower. This can be quantified by calculating the expected number of counts that maximizes the probability of finding seven objects in one field and one in the other. Out of 10,000 Monte Carlo realizations we find 0.40% of such cases, i.e., the significance of this overdensity is 99.6%.

The above estimates are based on the oversimplification that galaxies are not clustered. Here we evaluate our results based on the cosmic variance determined from a cosmological simulation. The expected number of galaxies is predicted from the cosmological smoothed particle hydrodynamics (SPH), cold dark matter (CDM) model of Choi, J. H. (2009, 2010). The simulated galaxies have appropriate colors and magnitudes, allowing us to make a direct comparison to our observation. In order to simulate galaxies at  $z = 7$ , we have applied (i) a bright magnitude cut at  $z_R > 24$ , and (ii) a detection completeness. Then, we count how many galaxies would be found in the field of view of Suprime-Cam. To evaluate the completeness of our detection procedure as a function of magnitude, we add artificial objects to the  $z_R$  image with all detected objects masked. The artificial objects are modeled by a Moffat function with a half light radius of 0.9 arcsec in the magnitude range of 24 to 25.46. We used the IRAF task “noao.artdata.mkobjects” for this procedure. Then, we repeat the object detection and measure the success rate.

After applying the completeness and magnitude cuts to the simulated data, we have a realistic sample that can be compared to our observational data. By randomly sampling the Suprime-cam size field of view from the simulation, we measured the galaxy frequency distribution (Fig. 5). Based on this simulation, we found that the probability to find one pointing with seven galaxies and another with one is less than 0.4%, in good agreement with the results from the Poissonian statistics detailed above. Our results suggest that it is hard to explain the overdensity by a chance coincidence of galaxies due to cosmic variance.

#### 4.4. Spatial distribution of the LBGs

In this subsection, we discuss the peculiar spatial distribution of the LBGs. Fig. 6 shows the spatial distribution of the  $z \sim 6.4$  galaxies. The cross located at the center indicates the position of CFHQS J2329-0301, and

Spatial distribution of LBGs around  $z=6.4$  QSO

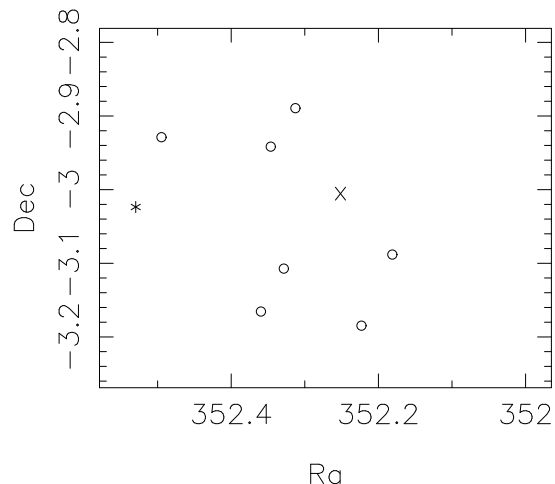


Fig. 6.— Spatial distribution of  $z > 6.4$  LBGs (circles), CFHQ J2329-0301 at  $z = 6.43$  (cross) and a newly identified QSO candidate (asterisk).

circles represent the  $z \sim 6.4$  galaxies. It appears that while these galaxies are clustered around the QSO, none are in its direct vicinity. (the closest galaxy being already at a (projected) distance of  $\sim 2$  Mpc from the QSO). To quantify the significance of this effect, we show a histogram of the angular distances from the QSO to each of the galaxies in Fig. 7 (red solid histogram). The distribution indeed suggests that there is a deficit of galaxies at  $< 2$  Mpc, while typical clustered distributions are expected to peak at the center. The blue dotted line in Fig. 7 is based on the positions of randomly distributed objects (but avoiding the masked regions just as in the real data). Comparing the two histograms suggests that in the QSO field the number of galaxies at the projected distance from 2 to 4 (physical) Mpc/h is indeed larger than that expected from a random distribution. We perform a Kolmogorov-Smirnov test by calculating the following value:

$$D = \max_i |R_i - M_i|, \quad (4)$$

where  $R_i$  is the number of galaxies in the  $i$ -th bin and  $M_i$  is the number in the same bin as given by the randomly distributed galaxies. We construct a histogram of the  $D$  statistic using 10000 times realizations, finding that the distribution in the QSO field differs from the random distribution at a 97% confidence level. If we just compare the peak at 3 Mpc, it has a  $1.7 \sigma$  excess over the random distribution.

#### 4.5. Evidence for additional QSOs?

Finally, we search for additional QSOs in the field by applying a set of color-color criteria tuned to the colors expected for QSOs at  $z \sim 6.4$ . Since a QSO continuum decreases with wavelength blue-ward of  $\text{Ly}\alpha$ , a QSO will have  $i' - z' > 1.9$  and  $z' - z_R < 0.3$  (Fig. 1). Note that this is a different (bluer) cut than that used for galaxies. We apply these criteria to all objects detected at  $> 3\sigma$  in all bands and having a FWHM smaller than 0.65 arcsec (equal to  $\text{FWHM} + \sigma_{\text{FWHM}}$ ). We found two objects (see Table 2). One of these is CFHQS J2329-0301, showing that our QSO selection works. Although the redshift

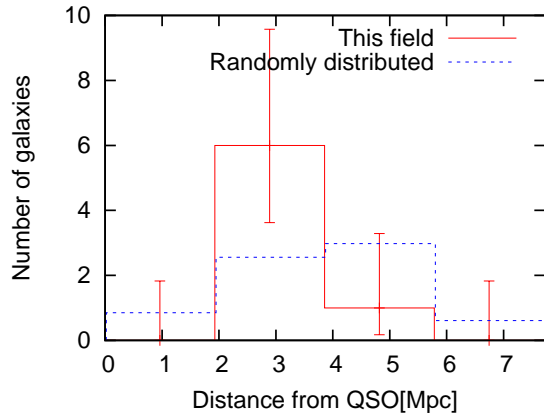


FIG. 7.— Histogram of radial distances (in projected, physical Mpc) from the QSO to each of the galaxies (red line). The blue dashed line was derived by taking the average of 100 realizations of a randomly distributed population having the same number of galaxies. Error bars indicate the 1 sigma poisson error using Eqn. (9) and Eqn (13) from Gehrels (1986). We find a  $1.7\sigma$  excess in the number of galaxies at a distance of  $\sim 3\text{Mpc}/h_{70}$ . Interestingly, this distance is similar to the size of the HII region around  $z \sim 6$  QSO (Wyithe et al. 2005).

TABLE 2  
A NEW QSO CANDIDATE FOUND BASED ON COLOR-COLOR SELECTION.

id	$\alpha_{2000}$	$\delta_{2000}$	$z_R$	$i' - z'$	$z' - z_R$	FWHM
8	23:30:14.95	-03:03:17.1	19.45	3.26	0.14	0.60
CFHQS	23:29:08.28	-03:01:58.2	21.76	4.11	-0.39	0.57

and nature of the second object must be confirmed with spectroscopy, it may be another QSO associated with the structure of galaxies surrounding CFHQS J2329-0301. If so, this would add supporting evidence that this field is relatively overdense. The position of the QSO candidate is indicated by the asterisk in Fig.6.

## 5. DISCUSSION

We found an overdensity of LBGs around the QSO with a 99.6% significance. We furthermore found evidence for a ring-shaped distribution, albeit at the  $< 2$  sigma level. Although the physical interpretation must await verification using deeper data or spectroscopic follow-up, below we will discuss possible physical interpretations under the assumption that our results are significant and represent real structure surrounding the QSO.

### 5.1. Comparison with previous work

At lower redshift, the environments of QSOs and fainter AGN have been extensively studied. At  $0.05 < z < 0.095$ , Miller et al. (2003) found that the fraction of galaxies with an AGN is independent of the local galaxy density, in a stark contrast to both star-forming and passive galaxies that show an environmental dependence (e.g., Goto et al. 2003). Lietzen et al. (2009) found an underdensity of bright galaxies at a few Mpc scale from nearby QSOs at  $0.078 < z < 0.172$ . Kauffmann et al. (2004) found that at fixed stellar mass the number of galaxies that host active galactic nuclei (AGNs) with strong [O III] emission indicating strong AGN activity is twice as high in low-density regions compared to high

density regions at  $0.04 < z < 0.06$ .

However the situation is different at higher redshifts. A Keck survey of fields centered on known  $z > 4$  QSOs found excesses in the number of companion galaxies (Djorgovski 1999). Kashikawa et al. (2007) found that LBGs without Ly $\alpha$  emission form a filamentary structure near a QSO at  $z \sim 5$ , while Ly $\alpha$  emitters are distributed around it but avoid it within a distance of  $\sim 4.5$  Mpc. Miley et al. (2004) also found that LBGs are concentrated around a luminous radio galaxy at  $z \approx 4.1$  previously found to be associated with an overdensity of  $\sim 30$  spectroscopically confirmed Ly $\alpha$  emitters (Venemans et al. 2007, 2002). In Overzier et al. (2006, 2008) it was shown that the environments of some radio galaxies at  $z = 4 - 5$  appear richer than the average field at  $\sim 3 - 5\sigma$  significance based on a detailed comparison with GOODS. However, these studies found no difference between the physical properties of galaxies in protoclusters compared to those in the field.

The difference between the low- $z$  and high- $z$  environments of AGN perhaps stems from the different halo masses that host them. Due to the flux limited nature of observational surveys, high- $z$  QSOs are much more luminous than local AGNs, and thus, presumably embedded in a more massive halo. Indeed, a generic expectation in most models of galaxy formation is that the most massive density peaks in the early universe (such as QSOs and massive galaxies) are likely to be strongly clustered (Kaiser 1984; Efstathiou & Rees 1988). In the hierarchical formation and evolution scenario of galaxies and QSOs (Haehnelt & Kauffmann 2000), luminous QSOs are located in rare overdense regions. This is why high- $z$  QSOs have been used as beacons to search for high density regions (Coldwell & Lambas 2006). Croom et al. (2005) and Shen et al. (2007) found an increasing clustering of QSOs with redshift.

Surprisingly, at  $z > 6$  the situation appears to change again; luminous QSOs are not necessarily found in strong density peaks. Kim et al. (2009) studied the number densities of  $i$ -dropout objects around 5 SDSS  $z \sim 6$  QSOs using the HST/ACS. They found an overdensity in two fields and underdensity in two fields. Zheng et al. (2006) and Stiavelli et al. (2005) found an overdensities around the QSOs SDSSJ0836+0054 ( $z = 5.82$ ) and SDSS J1030+0524 ( $z = 6.28$ ). However, these overdensities do not appear to be as magnificent structures as were found at lower redshift, or even in some random regions at  $z \sim 5 - 6$  (e.g., Ouchi et al. 2004b; Kashikawa et al. 2007; Ota et al. 2008).

One of the major problems of previous work at  $z \sim 6$  is the relatively small FoV of the HST/ACS. The  $200'' \times 200''$  field can only probe a region of  $1 \text{ Mpc} \times 1 \text{ Mpc}$  at  $z \sim 6$ , and thus may easily miss any larger structures such as found in this work. Computer simulations also predict that the largest structures present at  $z \sim 6$  span several tens of Mpc (Overzier et al. 2009), while LFs of LBGs show a large field-to-field variation (Hu et al. 2004; Ouchi et al. 2009). These results suggest that previous non-detections of overdensities around QSOs may need to be re-examined using a larger field of view or deeper observations. The difference in the FoV is perhaps the primary reason why no previous work has detected a highly significant overdensity around any of the  $z \sim 6$  QSOs. Our positive detection may have been

facilitated by the large field of view that allowed us to investigate the structure at scale of  $\sim 3$  Mpc.

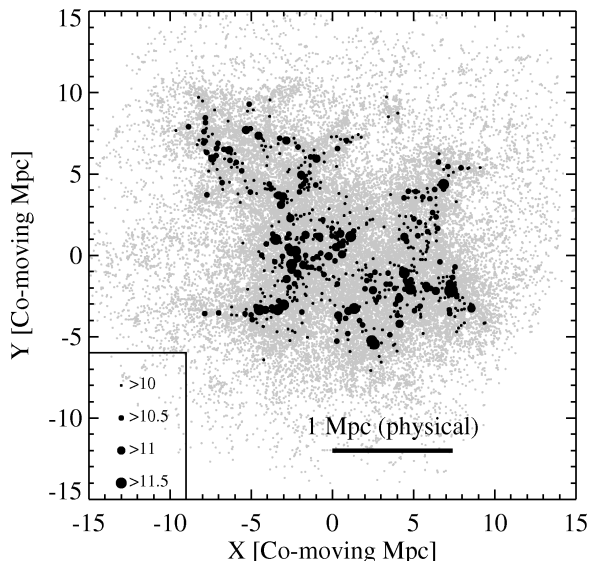


FIG. 8.— Illustration of a massive protocluster region selected from a large cosmological  $N$ -body simulation. The protocluster region shown is the progenitor of the most massive cluster found in the *Millennium-II Simulations* (corresponding to a  $M \simeq 10^{15} M_{\odot}$  cluster at  $z = 0$ ). Symbols show the (projected) distribution of dark matter halos having masses as indicated in the figure legend (values indicate the logarithm of the halo mass in  $M_{\odot}$ ). The scale bar indicates a physical radius of 1 Mpc.

For an illustration of what such a region at  $z \gtrsim 6$  might look like, we show an example of a large protocluster selected from the *Millennium-II* cosmological  $N$ -body simulations (Boylan-Kolchin et al. 2009). Figure 8 shows the (projected) spatial distribution of strongly clustered dark matter halos associated with a protocluster at  $z = 6.2$ . This protocluster is the progenitor of the most massive cluster found in the *Millennium-II* simulations, and corresponds to a  $M \simeq 10^{15} M_{\odot}$  cluster when evolved to  $z = 0$ . Figure 8 shows, at least qualitatively, that we may expect significant enhancements in the density of the galaxies that are hosted by the dark matter halos shown, provided that QSOs indeed trace protoclusters. A more quantitative analysis of the surface density of  $z$ -dropout galaxies near QSOs expected in the simulations is needed for a proper comparison.

### 5.2. Size of the HII region

Next, we compare our finding of an overdensity of LBGs around a QSO at a characteristic scale of 3 Mpc to spectroscopic measurements of HII regions around QSOs.

It has been demonstrated through spectroscopic observations that there exist large, ionized regions around luminous QSOs. These are sometimes called HII regions, Stromgren spheres, or highly ionized near zones. In this work, we will refer to them as HII regions. In order to define the size of the HII region, Fan et al. (2006b) proposed a definition as a point in the spectra where the Ly $\alpha$  transmission first drops to  $T < 0.1$  for spectra binned in 20 $\text{\AA}$  pixels. The CFHQS J2329-0301 transmission drops at  $T < 0.1$  first at 3.6 Mpc, then again at 6.3 Mpc (Willott et al. 2007). Interestingly, the size of this spectroscopically measured HII region is comparable

to the possible ring shape distribution of LBGs around CFHQS2329-0301 (Fig. 6). Note that the size of the spectroscopic HII region is expected to be larger ( $\sim 10$  Mpc) for the SDSS QSOs due to their higher luminosities (they are brighter by  $\sim 2$  mag). In addition to the small FoV of HST/ACS, this may be an additional reason, why no significant overdensity of LBGs has been found around SDSS QSOs. To observe an overdensity of galaxies at a scale of  $>10$  Mpc (such as expected around the luminous SDSS QSOs at  $z \sim 6$ ), one needs multiple FoVs even with the Suprime-Cam. We conclude that the size of the HII region is consistent with the apparent lack of LBG candidates closest to the QSO.

### 5.3. Possible Physical Mechanisms

If our detection of the lack of LBGs near the QSO is real, then, what created the observed paucity of galaxies within 3 Mpc from the QSO? One possibility is that the intense emission of ionizing radiation associated with QSOs ionizes the surrounding IGM and may even photoevaporate the gas in neighboring dark halos before it has the opportunity to cool and form stars. In this scenario, QSOs would suppress galaxy formation in their vicinity. One would then observe a paucity of galaxies near a QSO despite the underlying excess of dark matter halos. Shapiro et al. (2004) presented the first theoretical simulations of the gas dynamics coupled with radiative transfer, showing that an ionizing source that emits  $10^{56}$  photons  $\text{s}^{-1}$  (appropriate for a QSO) can indeed photoevaporize minihalos of  $\sim 10^7 M_{\odot}$  (that would have been able to form small galaxies) on 100–150 Myr timescales (but see Barkana & Loeb 1999; Wyithe et al. 2005). Compared with our observational results of finding a “ring”-shaped distribution of LBGs, the central QSO may have suppressed the formation of surrounding galaxies thereby creating a paucity of galaxies in its vicinity but still having an overdense region beyond the inner, ionized region. This may explain the observed results, at least qualitatively.

However, Kashikawa et al. (2007) quantitatively estimated that such UV radiation from QSO can suppress galaxy formation or not. According to their simulation, QSO UV radiation can suppress star formation in a halo with  $M_{\text{vir}} < 10^9 M_{\odot}$ , while a halo with  $M_{\text{vir}} > 10^{11} M_{\odot}$  is unaffected. Although mass estimate of our  $z \sim 6.4$  LBG are uncertain because we do not have deep near-infrared data, considering bright magnitude, they are likely to be massive galaxies with  $M_{\text{vir}} \sim 10^{11-12} M_{\odot}$ . If so, QSO UV radiation is not strong enough to create the central deficit we observed.

Can we find other theoretical predictions that could explain the observations? The simulation of Kashikawa et al. (2007) assumed star formation in spherical dark matter halos. They found that the impact of photoionization is greater if that star formation is taking place in a disk or in substructures (which is perhaps likely to be the case). If the QSO formed at a much earlier time than the surrounding galaxies, this scenario might be able to suppress the formation of galaxy seeds at the time when their masses were still sufficiently small.

Another plausible scenario is that the IGM surrounding the QSO may have been ionized by galaxies long before the QSO turned on. It has been suggested that because luminous QSOs are expected to form in rare over-

dense regions, the surrounding IGM had already been pre-ionized by galaxies (Yu & Lu 2005). According to the simulation of Bolton & Haehnelt (2007), the neutral hydrogen fraction,  $f_{HI}$ , near a QSO is estimated to be  $f_{HI} < 0.3$ . Therefore, QSO radiation is emitted into a substantially pre-ionized IGM. In this case, galaxies that formed before the QSO started emitting its strong UV radiation may still be present in the vicinity of the QSO. Because such galaxies are likely to have ceased their star formation, they would not be detected by our LBG technique.

In an overdense region, the QSO host galaxy is likely to be the most massive galaxy that formed the earliest. According to Yu & Lu (2005), QSO host galaxies experiencing rapid star formation at a rate of  $\sim 3000 M_{\odot} \text{ yr}^{-1}$  combined with the radiation field emitted by the QSO itself can produce enough photons to ionize a large HII region. In order to check whether we see any evidence for the presence of such a massive host galaxy, we have performed a careful PSF subtraction on our images. The residuals indicate the detection of a large host galaxy by SED fitting ( $R_e=11\text{kpc}$ ,  $\lesssim 10^{10} M_{\odot}$ ) associated with the QSO CFHQS J2329-0301 (Goto et al. 2009) with evidence of extensive star formation based on its extended rest-frame UV flux. The presence of a massive host galaxy may thus support a scenario in which the QSO and its host galaxy evolve together, suppressing galaxy formation in their vicinity.

Alternatively, it has also been suggested by Dijkstra et al. (2008) that in order to facilitate the formation of a supermassive black hole by  $z \sim 6$  in the first place, it may be required to have a rare pair of dark matter halos in which the intense UV radiation from one halo prevents fragmentation of the other, so that the gas collapses directly into a supermassive black hole, and explaining the lack of galaxies forming in its vicinity as observed in our field. Consistent with this scenario, it is interesting to note that we found a second QSO candidate located near the eastern edge of the field (see §4.4). We speculate that this could be a QSO associated with the adjacent (second) halo that ionized the original halo.

Last, it has been suggested that a  $z \sim 6$  QSO is likely to have experienced multiple mergers in order for its black hole to grow to a mass of  $\sim 10^9 M_{\odot}$ . An example of this scenario is given by the simulation of Li et al. (2007), which predicts that the host galaxy of a  $z \sim 6$  QSO may have experienced seven mergers with mass ratios of 4:1 or greater (see their Fig. 3). The QSO in our field may thus have merged with all the galaxies in its direct vicinity, explaining the peculiar spatial distribution that we find. This is also consistent with the discovery of the large host galaxy associated with the QSO (Goto et al. 2009).

In summary, although our detection of substructure in the LBG distribution near the QSO is rather weak ( $\lesssim 2\sigma$ ), studies of the spatial distribution of LBGs around QSOs at  $z \sim 6$  are very important for testing numerous of the interesting physical scenarios related to the co-evolution of QSOs and galaxies as discussed above. Therefore, it is important that our conclusions are verified using deeper, multi-wavelength imaging and spectroscopic observations that may detect additional galaxies

missed by our current selection, such as galaxies that are below our (UV) detection limits, star-forming galaxies that are heavily obscured, or galaxies in which star formation has ceased. Also, it will be important to extend the analysis performed here to other fields to obtain good statistics on the typical structures associated with QSOs at this extreme redshift.

## 6. CONCLUSIONS

Taking advantage of the large field of view ( $34' \times 27'$ ) and the new red-sensitive fully depleted CCDs recently installed on the Subaru/Suprime-Cam, we have investigated the large scale environment around the most distant QSO studied to date.

Our findings are as follows. The number of candidate LBGs at  $z \sim 6.4$  is 7 times larger than that in a comparison field (the Subaru Deep Field), suggesting that the QSO field hosts an overdense region. We estimate that the probability that this overdensity is a chance coincidence is less than 0.4% based on either using simple Poissonian statistics, or on a comparison with a cosmological SPH simulation of  $z \sim 7$  galaxies.

We find evidence for a non-uniform distribution of the LBGs in a “ring-like” shape surrounding the QSO at a radius of  $\sim 3$  physical Mpc, i.e., galaxies are overdense around the QSO, but at the same time they avoid the very center near the QSO (see Figs. 6 and 7). A KS-test shows that the radial distribution of LBGs in Fig. 7 is different from random at a 98% significance level. The distance of 3 Mpc is comparable to the size of the HII region around QSOs at  $z \sim 6$  (Wyithe et al. 2005). Possible physical explanations of such a central deficit of galaxies include the suppression of galaxy formation due to the strong UV radiation field of the QSO. However, because the significance of our detection of a non-uniform distribution of LBGs around the QSO is low, it is important to verify these results with deeper imaging data and/or spectroscopy.

Our findings show that QSOs at  $z \sim 6$  may indeed be embedded in the densest regions of the early universe, provided that they are observed on significantly larger scales compared to previous studies that used the relatively small field of view provided by HST.

## 7. ACKNOWLEDGMENTS

We thank the anonymous referee for careful reading of the manuscript and many insightful suggestions. We are grateful to K. Shimasaku and M. Ouchi for providing  $z_R$  filter, valuable comments and a careful reading of this paper and also thank N. Asami for providing valuable comments. We thank Jason Jaacks, Jun-Hwan Choi, and Kentaro Nagamine for providing us with the results of their cosmological hydrodynamic simulation.

Y.U. acknowledges grant aid for large storage system from the Department of Astronomical Sciences of the Graduate University for Advanced Studies (SOK-ENDAI). T.G. acknowledges financial support from the Japan Society for the Promotion of Science (JSPS) through JSPS Research Fellowships for Young Scientists.

The Millennium-II Simulation databases used in this paper and the web application providing online access to them were constructed as part of the activities of the German Astrophysical Virtual Observatory.

The authors wish to recognize and acknowledge the

very significant cultural role and reverence that the summit of Mauna Kea has always had within the indigenous Hawaiian community. We are most fortunate to have

the opportunity to conduct observations from this sacred mountain.

## REFERENCES

- Abazajian, K., & Sloan Digital Sky Survey, f. t. 2008, ArXiv e-prints
- Barkana, R., & Loeb, A. 1999, *ApJ*, 523, 54
- Bertin, E. 2006, in *Astronomical Society of the Pacific Conference Series*, Vol. 351, *Astronomical Data Analysis Software and Systems XV*, ed. C. Gabriel, C. Arviset, D. Ponz, & S. Enrique, 112–+
- Bertin, E., & Arnouts, S. 1996, *A&AS*, 117, 393
- Bolton, J. S., & Haehnelt, M. G. 2007, *MNRAS*, 381, L35
- Boylan-Kolchin, M., Springel, V., White, S. D. M., Jenkins, A., & Lemson, G. 2009, *MNRAS*, 398, 1150
- Bruzual, G., & Charlot, S. 2003, *MNRAS*, 344, 1000
- Caballero, J. A., Burgasser, A. J., & Klement, R. 2008, *A&A*, 488, 181
- Chiu, K., Fan, X., Leggett, S. K., Golimowski, D. A., Zheng, W., Geballe, T. R., Schneider, D. P., & Brinkmann, J. 2006, *AJ*, 131, 2722
- Choi, J. H. & Nagamine, K., 2009, *MNRAS*, 393, 1595
- Choi, J. H. & Nagamine, K., 2010, *MNRAS*, in press
- Coldwell, G. V., & Lambas, D. G. 2006, *MNRAS*, 371, 786
- Croom, S. M., Boyle, B. J., Shanks, T., Smith, R. J., Miller, L., Outram, P. J., Loaring, N. S., Hoyle, F., & da Ángela, J. 2005, *MNRAS*, 356, 415
- Dijkstra, M., Haiman, Z., Mesinger, A., & Wyithe, J. S. B. 2008, *MNRAS*, 391, 1961
- Djorgovski, S. G. 1999, in *Astronomical Society of the Pacific Conference Series*, Vol. 193, *The Hy-Redshift Universe: Galaxy Formation and Evolution at High Redshift*, ed. A. J. Bunker & W. J. M. van Breugel, 397–+
- Djorgovski, S. G., Stern, D., Mahabal, A. A., & Brunner, R. 2003, *ApJ*, 596, 67
- Efstathiou, G., & Rees, M. J. 1988, *MNRAS*, 230, 5P
- Fan, X., Carilli, C. L., & Keating, B. 2006a, *ARA&A*, 44, 415
- Fan, X., Strauss, M. A., Becker, R. H., White, R. L., Gunn, J. E., Knapp, G. R., Richards, G. T., Schneider, D. P., Brinkmann, J., & Fukugita, M. 2006b, *AJ*, 132, 117
- Furusawa, H., Kosugi, G., Akiyama, M., Takata, T., Sekiguchi, K., Tanaka, I., Iwata, I., Kajisawa, M., Yasuda, N., Doi, M., Ouchi, M., Simpson, C., Shimasaku, K., Yamada, T., Furusawa, J., Morokuma, T., Ishida, C. M., Aoki, K., Fuse, T., Imanishi, M., Iye, M., Karoji, H., Kobayashi, N., Kodama, T., Komiyama, Y., Maeda, Y., Miyazaki, S., Mizumoto, Y., Nakata, F., Noumaru, J., Ogasawara, R., Okamura, S., Saito, T., Sasaki, T., Ueda, Y., & Yoshida, M. 2008, *ApJS*, 176, 1
- Gehrels, N. 1986, *ApJ*, 303, 336
- Golimowski, D. A., Leggett, S. K., Marley, M. S., Fan, X., Geballe, T. R., Knapp, G. R., Vrba, F. J., Henden, A. A., Luginbuhl, C. B., Guetter, H. H., Munn, J. A., Canzian, B., Zheng, W., Tsvetanov, Z. I., Chiu, K., Glazebrook, K., Hoversten, E. A., Schneider, D. P., & Brinkmann, J. 2004, *AJ*, 127, 3516
- Goto, T., Okamura, S., Sekiguchi, M., Bernardi, M., Brinkmann, J., Gómez, P. L., Harvanek, M., Kleinman, S. J., Krzesinski, J., Long, D., Loveday, J., Miller, C. J., Neilsen, E. H., Newman, P. R., Nitta, A., Sheth, R. K., Snedden, S. A., & Yamauchi, C. 2003, *PASJ*, 55, 757
- Goto, T., Utsumi, Y., Furusawa, H., Miyazaki, S., & Komiyama, Y. 2009, *MNRAS*, 400, 843
- Gunn, J. E., & Stryker, L. L. 1983, *ApJS*, 52, 121
- Haehnelt, M. G., & Kauffmann, G. 2000, *MNRAS*, 318, L35
- Hu, E. M., Cowie, L. L., Capak, P., McMahon, R. G., Hayashino, T., & Komiyama, Y. 2004, *AJ*, 127, 563
- Kaiser, N. 1984, *ApJ*, 282, 374
- Kamata, Y., Miyazaki, S., Nakaya, H., Tsuru, T. G., Tsunemi, H., Miyata, E., Muramatsu, M., Suzuki, H., & Miyaguchi, K. 2008, in *Society of Photo-Optical Instrumentation Engineers (SPIE) Conference Series*, Vol. 7021, *Society of Photo-Optical Instrumentation Engineers (SPIE) Conference Series*
- Kashikawa, N., Kitayama, T., Doi, M., Misawa, T., Komiyama, Y., & Ota, K. 2007, *ApJ*, 663, 765
- Kauffmann, G., White, S. D. M., Heckman, T. M., Ménard, B., Brinchmann, J., Charlot, S., Tremonti, C., & Brinkmann, J. 2004, *MNRAS*, 353, 713
- Kim, S., Stiavelli, M., Trenti, M., Pavlovsky, C. M., Djorgovski, S. G., Scarlata, C., Stern, D., Mahabal, A., Thompson, D., Dickinson, M., Panagia, N., & Meylan, G. 2009, *ApJ*, 695, 809
- Knapp, G. R., Leggett, S. K., Fan, X., Marley, M. S., Geballe, T. R., Golimowski, D. A., Finkbeiner, D., Gunn, J. E., Hennawi, J., Ivezić, Z., Lupton, R. H., Schlegel, D. J., Strauss, M. A., Tsvetanov, Z. I., Chiu, K., Hoversten, E. A., Glazebrook, K., Zheng, W., Hendrickson, M., Williams, C. C., Uomoto, A., Vrba, F. J., Henden, A. A., Luginbuhl, C. B., Guetter, H. H., Munn, J. A., Canzian, B., Schneider, D. P., & Brinkmann, J. 2004, *AJ*, 127, 3553
- Li, Y., Hernquist, L., Robertson, B., Cox, T. J., Hopkins, P. F., Springel, V., Gao, L., Di Matteo, T., Zentner, A. R., Jenkins, A., & Yoshida, N. 2007, *ApJ*, 665, 187
- Lietzen, H., Heinämäki, P., Nurmi, P., Tago, E., Saar, E., Liivamägi, J., Tempel, E., Einasto, M., Einasto, J., Gramann, M., & Takalo, L. O. 2009, *A&A*, 501, 145
- Miley, G. K., Overzier, R. A., Tsvetanov, Z. I., Bouwens, R. J., Benítez, N., Blakeslee, J. P., Ford, H. C., Illingworth, G. D., Postman, M., Rosati, P., Clampin, M., Hartig, G. F., Zirm, A. W., Röttgering, H. J. A., Venemans, B. P., Ardila, D. R., Bartko, F., Broadhurst, T. J., Brown, R. A., Burrows, C. J., Cheng, E. S., Cross, N. J. G., De Breuck, C., Feldman, P. D., Franx, M., Golimowski, D. A., Gronwall, C., Infante, L., Martel, A. R., Menanteau, F., Meurer, G. R., Sirianni, M., Kimble, R. A., Krist, J. E., Sparks, W. B., Tran, H. D., White, R. L., & Zheng, W. 2004, *Nature*, 427, 47
- Miller, C. J., Nichol, R. C., Gómez, P. L., Hopkins, A. M., & Bernardi, M. 2003, *ApJ*, 597, 142
- Miyazaki, S., Hamana, T., Shimasaku, K., Furusawa, H., Doi, M., Hamabe, M., Imi, K., Kimura, M., Komiyama, Y., Nakata, F., Okada, N., Okamura, S., Ouchi, M., Sekiguchi, M., Yagi, M., & Yasuda, N. 2002a, *ApJ*, 580, L97
- Miyazaki, S., Komiyama, Y., Sekiguchi, M., Okamura, S., Doi, M., Furusawa, H., Hamabe, M., Imi, K., Kimura, M., Nakata, F., Okada, N., Ouchi, M., Shimasaku, K., Yagi, M., & Yasuda, N. 2002b, *PASJ*, 54, 833
- Ota, K., Iye, M., Kashikawa, N., Shimasaku, K., Kobayashi, M., Totani, T., Nagashima, M., Morokuma, T., Furusawa, H., Hattori, T., Matsuda, Y., Hashimoto, T., & Ouchi, M. 2008, *ApJ*, 677, 12
- Ouchi, M., Mobasher, B., Shimasaku, K., Ferguson, H. C., Fall, S. M., Ono, Y., Kashikawa, N., Morokuma, T., Nakajima, K., Okamura, S., Dickinson, M., Giavalisco, M., & Ohta, K. 2009, *ApJ*, 706, 1136
- Ouchi, M., Shimasaku, K., Okamura, S., Furusawa, H., Kashikawa, N., Ota, K., Doi, M., Hamabe, M., Kimura, M., Komiyama, Y., Miyazaki, M., Miyazaki, S., Nakata, F., Sekiguchi, M., Yagi, M., & Yasuda, N. 2004a, *ApJ*, 611, 660
- 2004b, *ApJ*, 611, 685
- Overzier, R. A., Bouwens, R. J., Cross, N. J. G., Venemans, B. P., Miley, G. K., Zirm, A. W., Benítez, N., Blakeslee, J. P., Coe, D., Demarco, R., Ford, H. C., Homeier, N. L., Illingworth, G. D., Kurk, J. D., Martel, A. R., Mei, S., Oliveira, I., Röttgering, H. J. A., Tsvetanov, Z. I., & Zheng, W. 2008, *ApJ*, 673, 143
- Overzier, R. A., Guo, Q., Kauffmann, G., De Lucia, G., Bouwens, R., & Lemson, G. 2009, *MNRAS*, 394, 577

- Overzier, R. A., Miley, G. K., Bouwens, R. J., Cross, N. J. G., Zirm, A. W., Benítez, N., Blakeslee, J. P., Clampin, M., Demarco, R., Ford, H. C., Hartig, G. F., Illingworth, G. D., Martel, A. R., Röttgering, H. J. A., Venemans, B., Ardila, D. R., Bartko, F., Bradley, L. D., Broadhurst, T. J., Coe, D., Feldman, P. D., Franx, M., Golimowski, D. A., Goto, T., Gronwall, C., Holden, B., Homeier, N., Infante, L., Kimble, R. A., Krist, J. E., Mei, S., Menanteau, F., Meurer, G. R., Motta, V., Postman, M., Rosati, P., Sirianni, M., Sparks, W. B., Tran, H. D., Tsvetanov, Z. I., White, R. L., & Zheng, W. 2006, *ApJ*, 637, 58
- Shapiro, P. R., Iliev, I. T., & Raga, A. C. 2004, *MNRAS*, 348, 753
- Shen, Y., Strauss, M. A., Oguri, M., Hennawi, J. F., Fan, X., Richards, G. T., Hall, P. B., Gunn, J. E., Schneider, D. P., Szalay, A. S., Thakar, A. R., Vanden Berk, D. E., Anderson, S. F., Bahcall, N. A., Connolly, A. J., & Knapp, G. R. 2007, *AJ*, 133, 2222
- Shimasaku, K., Ouchi, M., Furusawa, H., Yoshida, M., Kashikawa, N., & Okamura, S. 2005, *PASJ*, 57, 447
- Springel, V., White, S. D. M., Jenkins, A., Frenk, C. S., Yoshida, N., Gao, L., Navarro, J., Thacker, R., Croton, D., Helly, J., Peacock, J. A., Cole, S., Thomas, P., Couchman, H., Evrard, A., Colberg, J., & Pearce, F. 2005, *Nature*, 435, 629
- Stiavelli, M., Djorgovski, S. G., Pavlovsky, C., Scarlata, C., Stern, D., Mahabal, A., Thompson, D., Dickinson, M., Panagia, N., & Meylan, G. 2005, *ApJ*, 622, L1
- Vanden Berk, D. E. and Richards, G. T. and Bauer, A. and Strauss, M. A. and Schneider, D. P. and Heckman, T. M. and York, D. G. and Hall, P. B. and Fan, X. and Knapp, G. R. and Anderson, S. F. and Annis, J. and Bahcall, N. A. and Bernardi, M. and Briggs, J. W. and Brinkmann, J. and Brunner, R. and Burles, S. and Carey, L. and Castander, F. J. and Connolly, A. J. and Crocker, J. H. and Csabai, I. and Doi, M. and Finkbeiner, D. and Friedman, S. and Frieman, J. A. and Fukugita, M. and Gunn, J. E. and Hennessy, G. S. and Ivezi?, ?. and Kent, S. and Kunszt, P. Z. and Lamb, D. Q. and Leger, R. F. and Long, D. C. and Loveday, J. and Lupton, R. H. and Meiksin, A. and Merelli, A. and Munn, J. A. and Newberg, H. J. and Newcomb, M. and Nichol, R. C. and Owen, R. and Pier, J. R. and Pope, A. and Rockosi, C. M. and Schlegel, D. J. and Siegmund, W. A. and Smee, S. and Snir, Y. and Stoughton, C. and Stubbs, C. and SubbaRao, M. and Szalay, A. S. and Szokoly, G. P. and Tremonti, C. and Uomoto, A. and Waddell, P. and Yanny, B. & Zheng, 2001, *W. AJ*, 122, 549V
- Venemans, B. P., Kurk, J. D., Miley, G. K., Röttgering, H. J. A., van Breugel, W., Carilli, C. L., De Breuck, C., Ford, H., Heckman, T., McCarthy, P., & Pentericci, L. 2002, *ApJ*, 569, L11
- Venemans, B. P., Röttgering, H. J. A., Miley, G. K., van Breugel, W. J. M., de Breuck, C., Kurk, J. D., Pentericci, L., Stanford, S. A., Overzier, R. A., Croft, S., & Ford, H. 2007, *A&A*, 461, 823
- Willott, C. J., Delorme, P., Omont, A., Bergeron, J., Delfosse, X., Forveille, T., Albert, L., Reylé, C., Hill, G. J., Gully-Santiago, M., Vinten, P., Crampton, D., Hutchings, J. B., Schade, D., Simard, L., Sawicki, M., Beelen, A., & Cox, P. 2007, *AJ*, 134, 2435
- Wyithe, J. S. B., Loeb, A., & Carilli, C. 2005, *ApJ*, 628, 575
- Yagi, M., Kashikawa, N., Sekiguchi, M., Doi, M., Yasuda, N., Shimasaku, K., & Okamura, S. 2002, *AJ*, 123, 66
- Yu, Q., & Lu, Y. 2005, *ApJ*, 620, 31
- Zheng, W., Overzier, R. A., Bouwens, R. J., White, R. L., Ford, H. C., Benítez, N., Blakeslee, J. P., Bradley, L. D., Jee, M. J., Martel, A. R., Mei, S., Zirm, A. W., Illingworth, G. D., Clampin, M., Hartig, G. F., Ardila, D. R., Bartko, F., Broadhurst, T. J., Brown, R. A., Burrows, C. J., Cheng, E. S., Cross, N. J. G., Demarco, R., Feldman, P. D., Franx, M., Golimowski, D. A., Goto, T., Gronwall, C., Holden, B., Homeier, N., Infante, L., Kimble, R. A., Krist, J. E., Lesser, M. P., Menanteau, F., Meurer, G. R., Miley, G. K., Motta, V., Postman, M., Rosati, P., Sirianni, M., Sparks, W. B., Tran, H. D., & Tsvetanov, Z. I. 2006, *ApJ*, 640, 574